

# How well does ramped thermal oxidation quantify the age distribution of soil carbon? Assessing thermal stability of physically and chemically fractionated soil organic matter

Shane W. Stoner<sup>1,2</sup>, Marion Schrumpf<sup>1</sup>, Alison Hoyt<sup>3</sup>, Carlos A. Sierra<sup>1,4</sup>, Sebastian Doetterl<sup>2</sup>, Valier Galy<sup>5</sup>, Susan Trumbore<sup>1</sup>

<sup>1</sup>Biogeochemical Processes Department, Max Planck Institute for Biogeochemistry, Jena, 07745, Germany

<sup>2</sup>Department of Environmental Systems Science, ETH Zürich, Zürich, 8092, Switzerland

<sup>3</sup>Earth System Science, Stanford University, Stanford, 94305, USA

<sup>4</sup>Department of Ecology, Swedish University of Agricultural Sciences, Uppsala, SE-750 07, Sweden

<sup>5</sup>Woods Hole Oceanographic Institution, Woods Hole, 02543, USA

*Correspondence to:* Shane W. Stoner (sstoner@bgc-jena.mpg.de)

## **Abstract**

Carbon (C) in soils persists on a range of timescales depending on physical, chemical and biological processes that interact with soil organic matter (SOM) and affect its rate of decomposition. Together these processes determine the age distribution of soil C. Most attempts to measure this age distribution have relied on operationally defined fractions using properties like density, aggregate stability, solubility, or chemical reactivity. Recently, thermal fractionation, which relies on the activation energy needed to combust SOM, has shown promise for separating young from old C by applying increasing heat to decompose SOM. Here, we investigated radiocarbon (<sup>14</sup>C) and <sup>13</sup>C of C released during thermal fractionation to link activation energy to the age distribution of C in bulk soil and components previously separated by density and chemical properties. While physically and chemically isolated fractions had very distinct mean <sup>14</sup>C values, they contributed C across the full temperature range during thermal analysis. Thus, each thermal fraction collected during combustion of bulk soil integrates contributions from younger and older C derived from components having different physical and chemical properties but the same activation energy. Bulk soil and all density and chemical fractions released progressively older and more <sup>13</sup>C-enriched C with increasing activation energy, indicating that each operationally defined fraction itself was not homogeneous but contained a mix of C with different ages and degrees of microbial processing. Overall, we found that defining the full age distribution of C in bulk soil is best quantified by first separating particulate C prior to thermal fractionation of mineral-associated SOM. For the Podzol analyzed here, thermal fractions confirmed that ~95% of the mineral-associated organic matter (MOM) had a relatively narrow <sup>14</sup>C distribution, while 5% was very low in <sup>14</sup>C and likely reflected C from the < 2mm parent shale material in the soil matrix. After first removing particulate C using density or size separation, thermal fractionation can provide a rapid technique to study the age structure of MOM and how it is influenced by different OM-mineral interactions.

## 34 **1 Introduction**

36 Soil organic matter (SOM) consists of a complex and diverse collection of organic molecules containing C that can  
38 persist in soil for timescales ranging from hours to millennia (Schuur et al., 2016). Plant tissue chemistry, soil  
40 environmental conditions, soil mineral characteristics, physical aggregation, and microbial communities have all been  
42 demonstrated to impact the stability of SOM (Lehmann and Kleber, 2015; Basile-Doelsch et al., 2020; Kleber et al.,  
2021). These factors collectively influence the age of carbon (C) in SOM and the age of C in microbial respiration,  
making it challenging to link the timescales of OM stabilization and destabilization to the various mechanisms that  
allow C to persist in soils.

44 Measurement of soil radiocarbon ( $^{14}\text{C}$ ) has been used for decades to describe mean SOM ages. However, the mean  
46  $^{14}\text{C}$  values measured on bulk SOM integrate different pools and stabilization mechanisms and thereby obscure  
48 critical information on the distribution of SOM age. By combining timescales from years to millennia, interpretation  
of bulk  $^{14}\text{C}$  measurements is made more difficult due to integration of  $^{14}\text{C}$  from both natural sources affected by  
radioactive decay (natural  $^{14}\text{C}$ , integrating multiple centuries to millennia) and  $^{14}\text{C}$  produced by atomic weapons  
("bomb"  $^{14}\text{C}$ ) that reflect short-term cycling (annual to century) (Trumbore, 2000; Baisden and Canessa, 2013).  
Disentangling these signals is complex and requires the integration of  $^{14}\text{C}$  data with models to estimate SOM transit  
times and ages (Sierra et al., 2018; Metzler et al., 2018).

52 In an effort to better describe the distribution of age and cycling rates in bulk SOM, a number of physical and  
chemical fractionation methods have been developed to elucidate how the bulk  $^{14}\text{C}$  can be broken into pools with  
54 different amounts of  $^{14}\text{C}$  depending on physical or chemical characteristics (Trumbore et al., 1990; Paul et al., 1997;  
Castanha et al., 2008; Sollins et al., 2009; Lavallee et al., 2020). In particular, density fractionation, a method that  
56 separates SOM associated with denser minerals from low-density 'free' particulate organic matter (FPOM), has  
demonstrated success in distinguishing faster (low density) from slower (mineral associated) cycling C (Gregorich  
58 et al., 2006; Cotrufo et al., 2019; Heckman et al., 2022). However, mineral-associated organic matter (MOM)  
fractions themselves have been shown by many studies to be comprised of both faster and slower cycling C as  
60 evidenced by the change in  $^{14}\text{C}$  content after chemical extraction or oxidation (examples include Anderson and Paul,  
1984; Balesdent, 1987; Trumbore and Zheng, 1996; Jagadamma et al., 2010; Schrumpf et al., 2021) or from tracking  
62 bomb  $^{14}\text{C}$  into mineral fractions (examples include Trumbore, 1993; Torn et al., 1997; von Lützow et al., 2007, and  
more recently Schrumpf et al., 2013; Rasmussen et al., 2018; Heckman et al., 2018). Despite their widespread use  
64 and demonstrated utility for separating organic C by age as well as physical and chemical properties, most  
fractionation methods consume significant laboratory time and resources (Lavallee et al., 2020; Heckman et al.,  
66 2022). Further, some treatments, such as dense sodium polytungstate solution, remove C that cannot be easily  
recovered or analyzed for C or  $^{14}\text{C}$  content, meaning that the isotopic signature of removed C must be solved using  
68 mass balance constraints.

70 Ramped pyrolysis/oxidation (RPO), or thermal fractionation, is a relatively new method to functionally fractionate  
OM in sediments and soils (Rosenheim et al., 2008; Plante et al., 2013; Hemingway et al., 2017). This process  
72 applies increasing temperature of thermal decomposition as a proxy for the activation energy ( $E_a$ ) required to oxidize  
C, with the assumption that this provides a comparable measure of its resistance to decomposition in the soil  
74 environment. The result is a reproducible profile of  $\text{CO}_2$  released as a function of increasing temperature  
(thermogram), from which  $E_a$  distributions can be calculated (Hemingway et al., 2017). By collecting the  $\text{CO}_2$   
76 released over specified intervals as temperatures are continuously increased, “pools” of C with distinct thermal  
stability can be isolated, collected, and analyzed isotopically (Rosenheim and Galy, 2012). Because all C is released  
78 as  $\text{CO}_2$ , it is possible to characterize all of the C in a sample rather than inferring losses from analysis of the residual  
material. A further advantage of such “thermal fractionation” is that it can be compared with pyrolysis-GC/MS of  
80 SOM to evaluate how the chemistry of combusted SOM also changes with  $E_a$ . Previous studies have shown that the  
breakdown of lipids and polysaccharides releases C at lower temperatures, while thermal decomposition of phenolic  
82 and aromatic compounds dominate at higher temperatures (Quénéa et al., 2006; Grandy et al., 2009; Sanderman and  
Grandy, 2020). Thus, thermal fractionation has the potential to define the  $^{14}\text{C}$  (age) distribution of organic C and  
84 relate that to the  $E_a$  and chemistry of the OM in a soil sample.

86 Several studies have investigated soils using oxidative thermal fractionation (Plante et al., 2013; Grant et al., 2019;  
Hemingway et al., 2019). Compared to sediments, where these methods have been more widely applied, soil  
88 thermograms release a greater proportion of the total C over a narrower temperature range and have lower variation  
in age across thermal fractions (Hemingway et al., 2019). This may reflect a broader set of OM sources in sediments  
90 that can include eroded soil containing very old and highly processed C as well as fresh material from aquatic  
organisms.

92  
Typically, C released from both sediments and soils by thermal oxidation also increases in age with temperature of  
94 combustion, i.e.,  $E_a$ , confirming linkages between SOM persistence and the mechanisms of C stabilization (Plante  
et al., 2011; González-Pérez et al., 2012). However, different SOM stabilization mechanisms or local environments  
96 can complicate the interpretation of  $E_a$ -age relationships; for example, the same chemical compound sorbed to  
different mineral substrates can have very different activation energies (Feng and Simpson, 2008). Thermal  
98 oxidation of OM not associated with minerals, such as dissolved organic C (DOC), oxidizes at narrow but relatively  
high temperature ranges, possibly contributing young C at high temperatures that would be mixed with C released  
100 from mineral fractions at the same temperature (Grant et al., 2019; Hemingway et al., 2019). Given the wide range  
of  $^{14}\text{C}$  ages measured in various physical and chemical fractions, and the potential for recycling of C in soils through  
102 microbial processing, we expect some range of C age within each bulk soil thermal fraction.

104 Here, we apply oxidative thermal fractionation to SOM previously separated using physical (density) and chemical  
(extraction and oxidation) methods. Using mass balance approaches, we describe the contribution of each fraction  
106 to bulk soil thermograms and  $^{14}\text{C}$  signatures. We also present thermal fractionation results using a commercially

available instrument only recently applied to characterize SOM thermal stability distributions (Natali et al., 2020; Rennert and Herrmann, 2020, 2022). Our goals were to determine (1) the degree to which the physically and chemically separated fractions represent mixtures of OM with different activation energies and  $^{14}\text{C}$  distributions; (2) to determine the  $^{14}\text{C}$  distribution of C contained in physically or chemically separated fractions; (3) to assess the viability of thermal fractionation as an alternative to more time intensive lab methods in determining the  $^{14}\text{C}$  distribution of SOM.

## 114 **2 Methods**

### 116 **2.1 Site description and density fractionation**

116 Soil material used in this study was sampled from a Podzol developed on granitic parent material under spruce forest in central Germany (Schrumpf et al., 2013, 2021). This soil was selected because it was already known to have large differences in  $^{14}\text{C}$  content between density fractions (Schrumpf et al., 2021) and because of strong depth-dependent differences in stabilization processes in Podzol A and B horizons (De Coninck, 1980). Surface (0-10 cm) and subsoil (30-50 cm) samples were subjected to laboratory fractionations described in detail by Schrumpf et al. (2013). Briefly, soils first underwent density separation using dense sodium polytungstate solution (SPT) ( $1.6 \text{ g/cm}^3$ ). Suspended OM was separated from denser material that did not float using centrifugation. The floating free particulate OM (FPOM) fraction was collected and rinsed to remove remaining SPT solution. The sinking fraction was dispersed again in  $1.6 \text{ g cm}^{-3}$  solution and sonicated to disrupt aggregates, then centrifuged. After centrifugation, floating material from the supernatant was collected, rinsed, and designated as occluded particulate organic matter (OPOM). The remaining dense material in the sediment was repeatedly rinsed to remove SPT solution and is designated mineral associated organic matter (MOM).

128

### 128 **2.2 Chemical fractionation**

130 Two chemical fractionations were performed in parallel on the MOM fraction, as described by Schrumpf et al. (2021). The first subsample was extracted with NaF-NaOH to solubilize and remove all potentially de-sorbable SOM complexed with minerals through pH increase and competition with OH- and F- anions (Kaiser et al., 2007; Mikutta and Kaiser, 2011). Briefly, 125 mL of a NaF-NaOH solution was added to 25g MOM material, agitated overnight, and centrifuged. The supernatant was extracted, and an additional 125 mL of NaF-NaOH was added to repeat this process four times in total. Then, each extraction was filtered through glass fiber filters and combined. The remaining soil material was washed with deionized water and freeze-dried.

138 The second chemically treated MOM underwent strong oxidation in heated hydrogen peroxide ( $\text{H}_2\text{O}_2$ ) to isolate the most resistant and oldest OM (Helfrich et al., 2007; Jagadamma et al., 2010). In this procedure, 60 mL  $\text{H}_2\text{O}_2$  was added to a mixture of 2 g MOM and 20 mL deionized water. Samples were then heated and periodically stirred in a  $50^\circ\text{C}$  water bath for a total of 120 hours. Samples were then centrifuged, washed with deionized water, freeze dried, and homogenized with a ceramic ball mill.

### 2.3 Thermal fractionation and method development

144 Oxidative thermal fractionation of bulk SOM and physically and chemically separated fractions was performed using  
146 an Elementar soliTOC Cube carbon analyzer. Samples were not analyzed under pyrolytic conditions, as pyrolysis  
148 can produce charring artifacts, and  $^{14}\text{C}$  distributions have been shown to be comparable between operational modes  
150 (Williams et al., 2014; Grant et al., 2019). The design of the instrument used is very similar to those used in previous  
152 thermal fractionation publications (Rosenheim and Galy, 2012; Bianchi et al., 2015). Primarily, it consists of two  
154 ovens in sequence, a mechanical arm to hold and manipulate the sample container, and a non-dispersive infrared  
156 analyzer (NDIR) to measure the  $\text{CO}_2$  concentration in the gas exiting the ovens. The sample is introduced to the first  
oven, which is heated at a constant rate under a constant flow of carrier gas supplied through the sampler arm (78%  
 $\text{N}_2$ , 22%  $\text{O}_2$ ). The second oven contains a Pt catalyst held at  $800^\circ\text{C}$  that ensures all C released from the sample is  
oxidized to  $\text{CO}_2$ . The carrier gas then passes through a glass tube filled with brass wire at  $20^\circ\text{C}$  to remove HCl from  
acidified samples (note that no samples were acidified in this experiment) followed by a glass tube containing  
magnesium perchlorate to remove water vapor. Finally,  $\text{CO}_2$  concentration in the gas mixture is measured by the  
NDIR (DIN 19539).

158 Several additional procedures were required to adapt use of the commercial device for collection of C released by  
160 thermal fractionation. Due to the relatively large sample size ( $> 1\text{g}$  of dried soil or fraction) required to collect small  
162 thermal fractions with sufficient C for radiocarbon measurement, and the high flow rate of carrier gas in this  
164 instrument, samples with high C content (such as standards or FPOM/OPOM fractions) were diluted to  $\sim 2\%$  (by  
166 weight) C with pre-combusted sand ( $1000^\circ\text{C}$  for 10 hours) to prevent ignition and charring during heating. An  
artificial soil standard was analyzed with different sand dilutions to ensure that thermograms were not altered by  
dilution with sand (Fig. S1). Further, the sample oven was designed for rapid heating (up to  $110^\circ\text{C min}^{-1}$ ), and  
temperatures were observed to be less stable at slower heating rates. To reduce the cycles of on/off oven cycling  
while ensuring thermogram consistency (with sand dilution), samples were heated at  $15^\circ\text{C per minute}$ .

168 To collect  $\text{CO}_2$  for isotope analysis, a custom collection manifold was attached to the instrument outflow port (Figs.  
170 S2-S4). The manifold consists of parallel glass  $\text{CO}_2$  traps submerged in  $\text{LN}_2$  under vacuum. Exhaust gas released  
172 within a desired temperature range (thermal fraction) flows through a cold trap until the desired upper temperature  
is reached. Then, the trap is closed and the next opened to collect the next  $\text{CO}_2$  fraction. This process is repeated for  
each thermal fraction (F1 (first thermal fraction) –  $F_{\text{max}}$  (highest temperature thermal fraction), see Appendix tables  
1 and 2). A vacuum pump together with a capillary restriction upstream of the manifold was used to reduce the  
174 overall pressure in the manifold system to  $< 6\text{ mbar}$  to improve cryotrapping efficiency and to prevent condensation  
of  $\text{O}_2$  in the  $\text{LN}_2$  traps.

176 Traps with  $\text{CO}_2$  samples were subsequently transferred to a vacuum line where the  $\text{CO}_2$  was further purified (see  
178 below) and measured volumetrically for comparison (calibration) of the NDIR  $\text{CO}_2$  analysis. An aliquot was taken  
for analysis of  $\delta^{13}\text{C}$  using a modified gasbench inlet to a continuous flow IRMS (Wendeborg et al., 2013). In addition

180 to CO<sub>2</sub>, we noticed that nitrogen oxide gasses (including N<sub>2</sub>O<sub>3</sub>, which is dark blue when frozen) were visibly trapped.  
182 These gasses are produced by the reaction of N<sub>2</sub> and O<sub>2</sub> at high temperatures. As these, as well as S oxides that also  
184 freeze with CO<sub>2</sub> at liquid nitrogen temperatures, can cause graphitization failure, we used an additional purification  
186 procedure to remove them. An amount of sample CO<sub>2</sub> representing approximately 0.5 mg C was transferred  
188 cryogenically and then sealed under vacuum in a pre-combusted borosilicate tube containing ~50 mg CuO and ~10  
mg Ag (Hemingway et al., 2017) and baked at 525°C for one hour. Purified CO<sub>2</sub> released after breaking this tube  
was graphitized using zinc reduction (Xu et al., 2007) and measured at the Keck AMS lab at University of California  
Irvine. Resulting radiocarbon data are expressed as Fraction Modern (Fm).

190 Thermograms and activation energy ( $E_a$ ) were analyzed using the open-source “rampedpyrox” Python package  
(Hemingway, 2017; Hemingway et al., 2017). For each thermogram, a distributed  $E_a$  model derived from time-  
192 temperature C-release data is solved inversely to produce a continuous distribution of  $E_a$  (in kJ mol<sup>-1</sup>). It assumes a  
finite set of  $n$  components (thermal fractions, in order of increasing temperature, referred to as F1 -  $F_{max}$ , where  
194  $F_{max}$  is thermal  $F_n$ , the highest temperature range collected (Appendix tables 1 and 2) in superposition to construct  
the bulk soil  $E$  distribution. Each of these components can thus be mathematically assigned a mean  $E_a$  ( $\mu E$ ) and  
196 standard deviation ( $\sigma E$ ). Here, standard deviation describes the variance of distribution of  $E$ , or the heterogeneity of  
the bonding environment, within a thermal fraction or sample, rather than data variance. Thus, direct comparisons  
198 can be made between  $E$  distribution within a thermal fraction and its isotopic composition. However, it should be  
noted that such  $E_a$  descriptors derived from thermograms are not necessarily comparable to other methods of  
measuring  $E_a$  (Feng and Simpson, 2008; Hemingway et al., 2019).

200

### 3 Results

202 We describe data on SOM decomposition as a function of temperature, modeled  $E_a$ , and isotopic signatures of  
thermal fractions within and between density and chemical fractions and compare these to thermal fractionation of  
204 the bulk soil. To our knowledge, this was the first thermal fractionation procedure performed using a commercial C  
analyzer. Results on the performance and reliability of this setup to demonstrate the viability of this method for  
206 future researchers are presented in Supplemental Text 1.

208 **Table 1:** Summary information of bulk soil and fraction thermal stability and isotopic compositions, including activation energy indices. Fm = Fraction Modern <sup>14</sup>C

Depth	Fraction	Fraction			Whole Fraction Fm	Max Thermal Fm <sup>a</sup>	Min Thermal Fm <sup>a</sup>
		Percent of Total C	$\mu E$ (kJ mol <sup>-1</sup> )	$\sigma E$ (kJ mol <sup>-1</sup> )			
0-10 cm	Bulk Soil	-	134.1	14.2	0.997	1.048	0.751
0-10 cm	FPOM	8.7	133.5	15.3	1.080	1.102	1.067
0-10 cm	OPOM	6.2	135.3	14.0	0.992	1.040	0.968
0-10 cm	MOM	85.1	133.7	15.8	0.985	1.037	0.728
0-10 cm	NaF Res.	28.8	137.8	18.2	0.912	0.959	0.761
0-10 cm	H <sub>2</sub> O <sub>2</sub> Res.	13.5	136.3	12.8	0.859	0.868	0.781
30-50 cm	Bulk Soil	-	138.7	14.0	0.824	0.854	0.323
30-50 cm	FPOM	15.6	141.8	15.9	1.087	1.085	1.064
30-50 cm	OPOM	8.2	144.3	14.7	0.847	0.869	0.822
30-50 cm	MOM	76.3	137.9	16.1	0.786	0.791	0.230 <sup>b</sup>
30-50 cm	NaF Res.	29.9	137.9	24.7	0.713	0.798	0.562
30-50 cm	H <sub>2</sub> O <sub>2</sub> Res.	15.5	141.2	17.7	0.628	0.753	0.414

210

<sup>a</sup>: Maximum and minimum <sup>14</sup>C content collected via thermal fractionation within the sample

212 <sup>b</sup>: Value calculated by mass balance, +/- 0.02 Fm

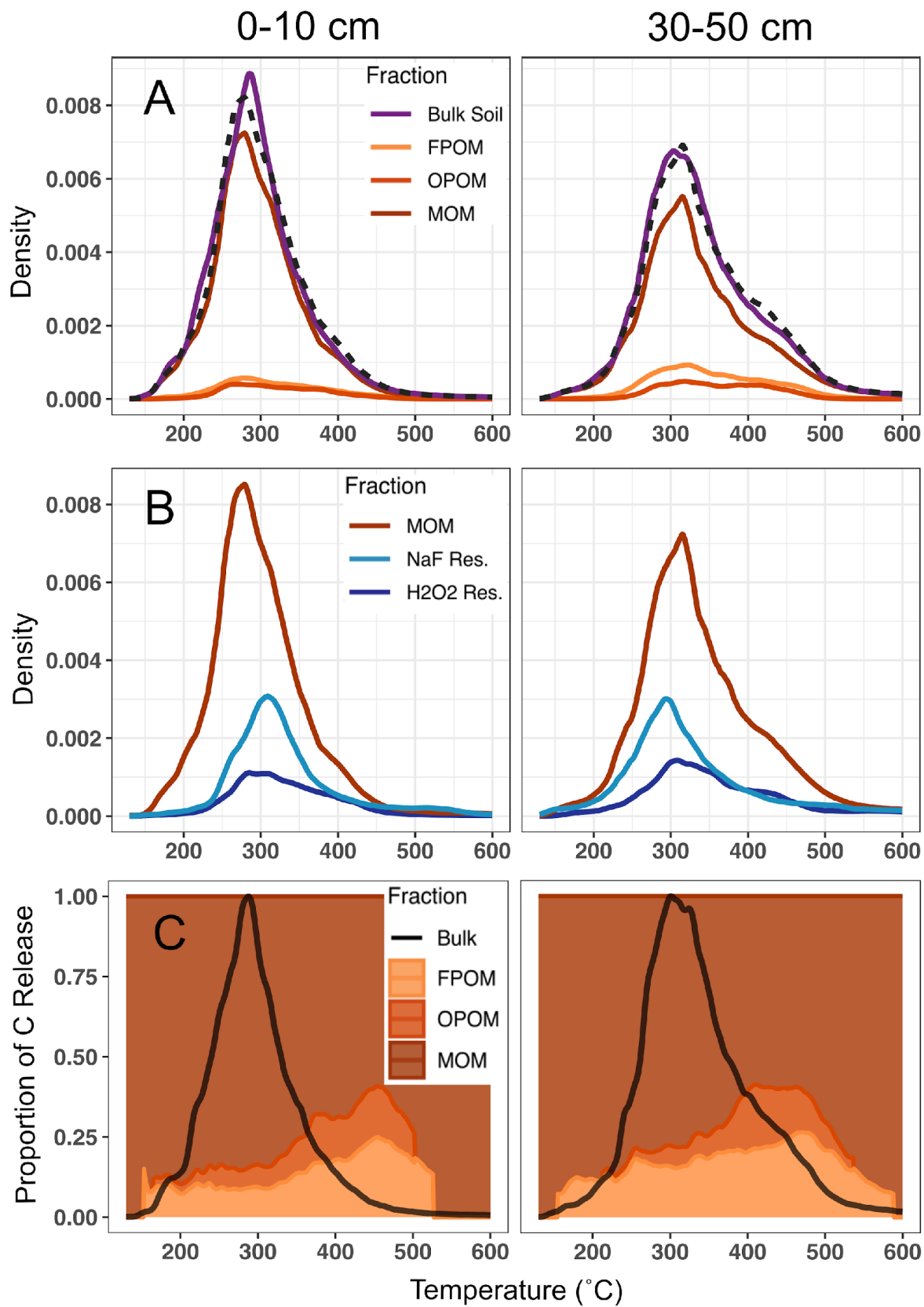
### 3.1 Thermograms and activation energy of physically and chemically fractionated organic matter

214 We compared the thermograms and the isotopic ( $^{14}\text{C}$  and  $^{13}\text{C}$ ) signatures of  $\text{CO}_2$  released as a function of temperature  
216 for each physical and chemical fraction individually, then compared the summed contribution of each  
218 physical/chemical fraction to the bulk soil (for density fractions) or MOM (for chemical fractions) to assess (1) the  
behavior of each of the different fractions and (2) how much each fraction contributes to the bulk thermogram at  
different temperature intervals.

220 All density and chemical fractions and bulk soil released 90-98% of their total C between 150 and 500°C. No fraction  
had a unique thermal signature (Figures 1a, 1b), and the thermograms mostly overlapped, with some C released  
222 across the whole temperature range of combustion. However, differences were observed among density fraction  
thermograms. For particulate fractions (FPOM and OPOM), C release displayed one or two muted peaks and most  
224 of the C was oxidized between 250 and 450°C. MOM and chemical residues released most of their C between 250  
and 350°C, but also released more C at temperatures >500°C compared to FPOM and OPOM fractions. Since most  
226 bulk soil C is in the MOM fraction (Table 1), thermograms for the bulk soil resemble those of the MOM fractions  
in both depths (Fig. 1a).

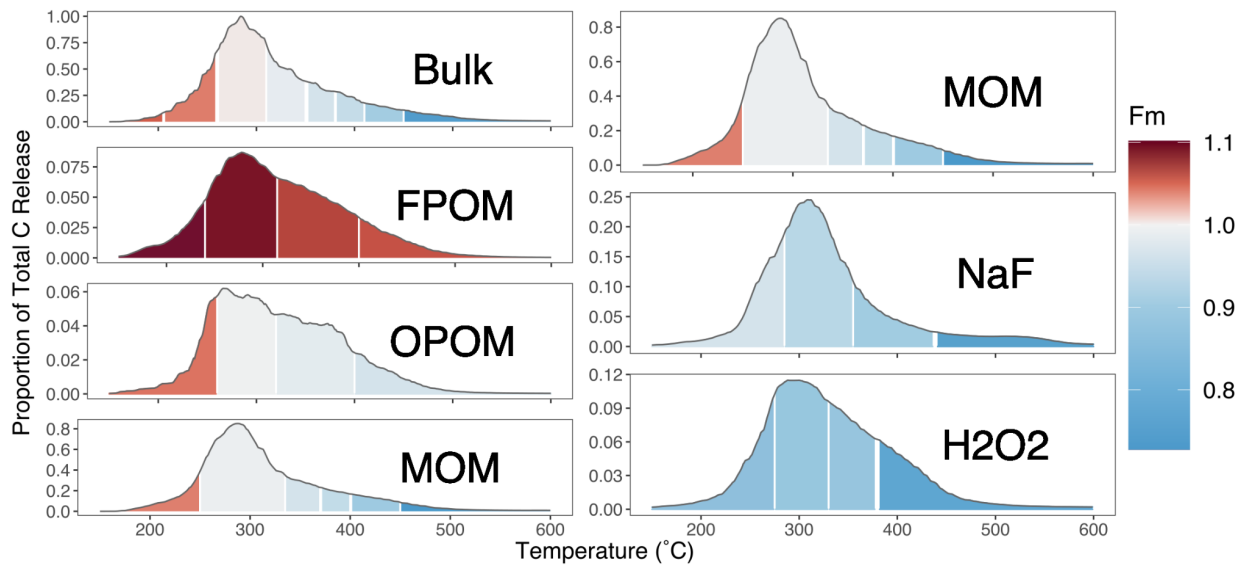
228 Mean activation energy ( $\mu E$ ) estimated from thermograms of bulk soil and fractions ranged from 133.5 to 137.8 kJ  
230  $\text{mol}^{-1}$  in surface soil and 137.9 to 144.3 kJ  $\text{mol}^{-1}$  in subsoil (Table 1, Appendix figs. 1 & 2, Appendix tables 1 & 2).  
Between depths,  $\mu E$  was greater in subsoil than surface soil on average by 5.2 kJ  $\text{mol}^{-1}$  ( $p = 0.01$ , paired  $t$ -test) for  
232 all samples except NaF extraction residues, which showed no difference. In subsoil, particulate fractions FPOM and  
OPOM  $\mu E$  values were ~3-6 kJ  $\text{mol}^{-1}$  greater than bulk soil and MOM but showed little difference in surface soils.  
234 Standard deviation of  $E$  ( $\sigma E$ ), a metric of bond strength heterogeneity, only varied with depth among chemical  
fraction residues which were ~5-6 kJ  $\text{mol}^{-1}$  greater in subsoil, suggesting greater diversity of bonds in the subsoil  
236 fractions (Hemingway et al. 2017). Thus, despite large differences in the chemistry and relationship to mineral  
surfaces, the  $E_a$  range was similar across all chemical and physical fractions. It is puzzling that NaF and  $\text{H}_2\text{O}_2$   
238 residues had lower activation energies than might be expected, given that they represent the most “recalcitrant” C  
resistant to harsh chemical treatments.

240

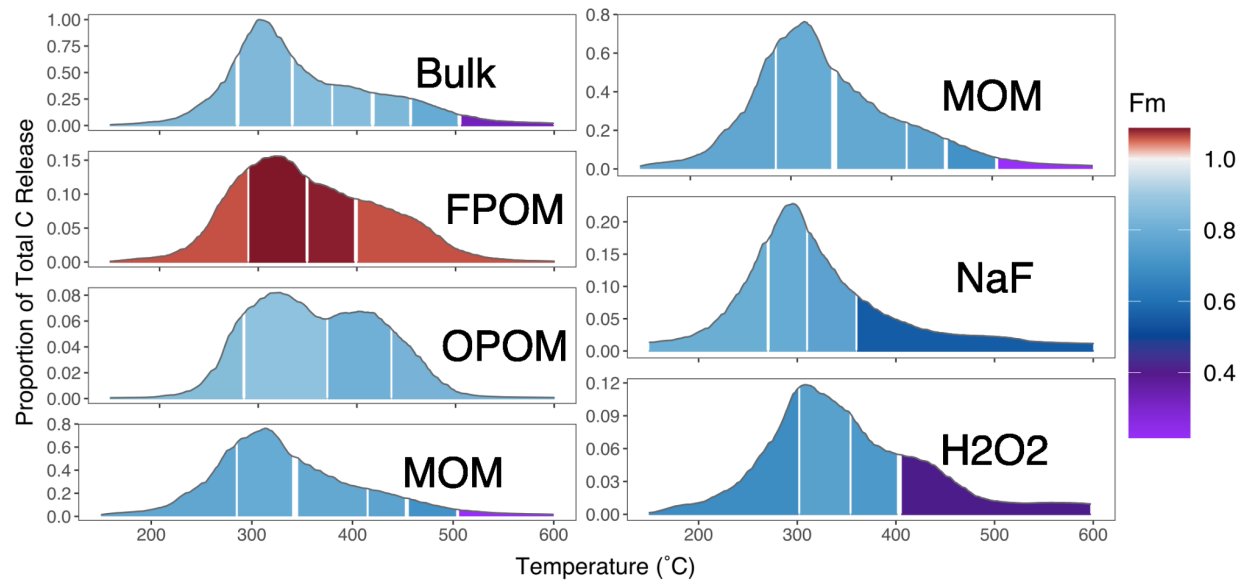


242 **Figure 1:** Relative magnitudes of thermograms, as C released as a function of temperature, with fractions scaled by  
their relative contribution to the total C in each panel. A: Bulk soil and density fraction thermograms, for 0-10 cm  
244 and 30-50 cm, respectively. Density fraction (FPOM, OPOM, MOM) thermograms are scaled to their relative  
contribution to total bulk soil C (Table 1). Dashed lines represent summed thermograms of the three density  
246 fractions. Comparison of summed and bulk thermograms show good agreement and suggest that fractionation  
procedures do not significantly alter the thermal stability of component fractions. B: Thermograms of MOM and  
248 chemical fractionation residues. The difference between MOM and given chemical fraction thermograms represent  
the thermal profile of C removed by the chemical treatment (NaF-NaOH or H<sub>2</sub>O<sub>2</sub>). Chemical fraction residue  
250 thermograms are scaled to their relative residual C content of the MOM fraction. C: Proportional contribution of  
density fractions to bulk soil C released across collection temperature range (colored fill). Solid black line represents  
252 bulk soil thermogram to highlight total C release from bulk soil at each temperature. Density fractions are cut off  
when C release is no longer discernible from instrument IR-detector background.

254



256

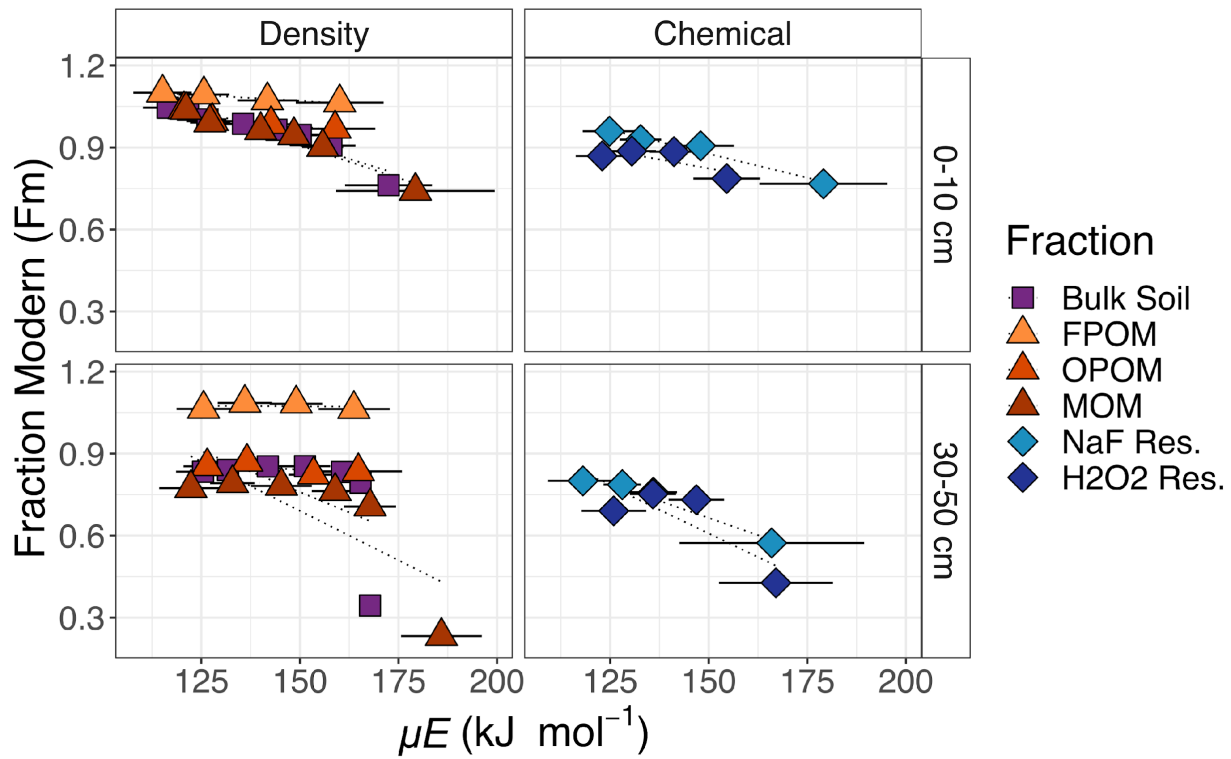


258

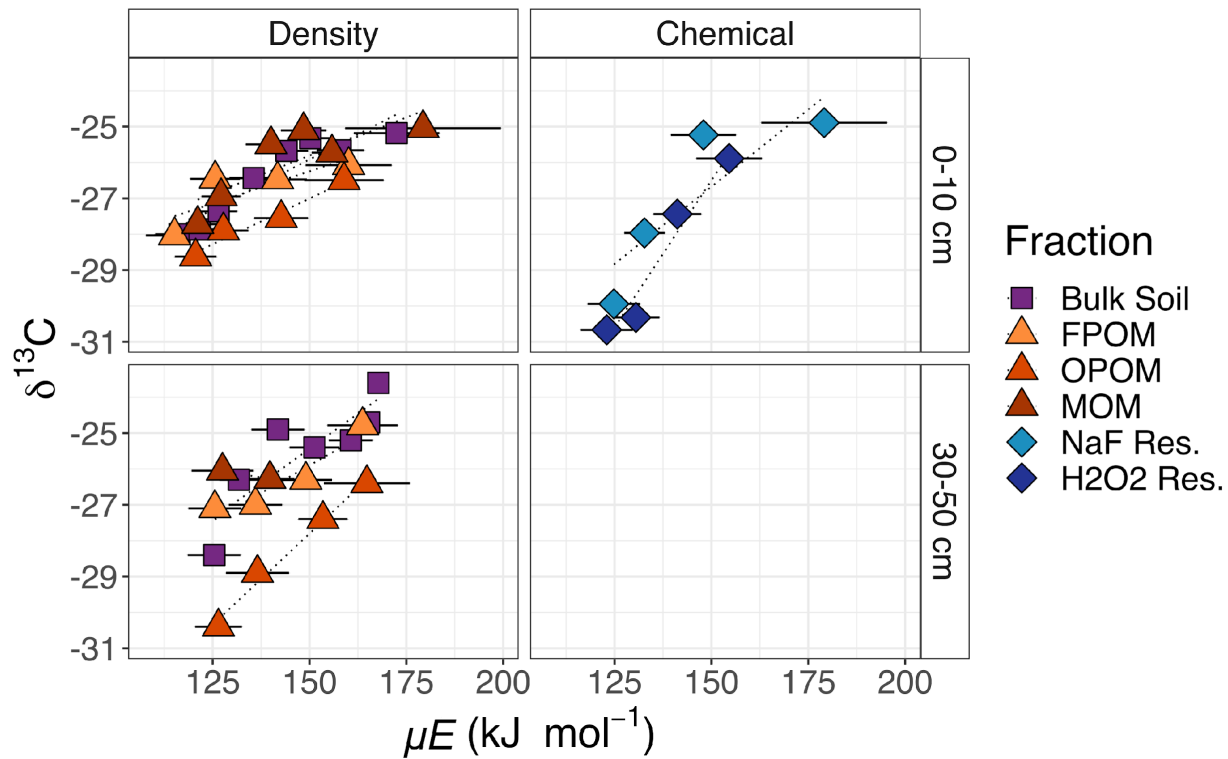
**Figure 2:** Thermograms with radiocarbon measurements. Top) 0-10 cm, Bottom) 30-50 cm. Left-hand column Y-axis values represent contribution to the total (bulk soil) C. NaF Res. and H2O2 Res. panels are scaled in proportion to their total C contribution to MOM. Color scale indicates the Fraction Modern (Fm) of the C released in each temperature range; the scale is doubled above Fm 1 to emphasize differences between post-bomb  $^{14}\text{C}$  ( $F_m > 1.0$ ) and  $^{14}\text{C}$  that has undergone significant radioactive decay ( $F_m < 1$ ).

260

262



264 **Figure 3:** Radiocarbon ( $F_m$ ) as a function of mean activation energy ( $\mu E$ ) for C collected across different temperature  
 intervals from combustion of bulk soil, compared with those of combusted component density and chemical fractions.  
 266 Horizontal bars represent  $\sigma E$  for each thermal fraction, which indicates the range of activation energies represented  
 by a given thermal fraction.



270 **Figure 4:**  $\delta^{13}\text{C}$  measured for each fraction as in Figure 3. Low C content and limited sample material prevented data  
 272 collection from some fractions (MOM, NaF Res.,  $\text{H}_2\text{O}_2$  Res. in subsoil). Right-hand labels denote depth in cm.

272

### 3.2 Radiocarbon

274 The mean radiocarbon ( $^{14}\text{C}$ , expressed as Fm) differed for each density or chemical residue fraction (Table 1). For  
 276 a given soil depth, the FPOM had the highest  $^{14}\text{C}$  content, consisting mostly of C fixed since the 1960's (Fm >1.0),  
 278 while the lowest  $^{14}\text{C}$  was in the residue after  $\text{H}_2\text{O}_2$  treatment of the MOM. The  $^{14}\text{C}$  of the bulk soil and each fraction  
 decreased from the 0-10 cm to 30-50 cm depth, and the overall pattern of Fm for the different physical and chemical  
 fractions (FPOM > OPOM > MOM > NaF residue >  $\text{H}_2\text{O}_2$  residue) remained the same.

280 Within all fractions, the Fm of released  $\text{CO}_2$  stayed similar or declined as the temperature increased (Figure 2;  
 282 temperatures of combustion are converted to  $E_a$  in Figure 3). In both Figures 2 and 3, the large differences in  $^{14}\text{C}$   
 284 between the FPOM other density and chemical fractions far exceed the range of Fm released across temperatures  
 during combustion of the individual fractions. Indeed, as reported by Schrupf et al. (2021), much of the combusted  
 C from MOM fractions had very similar  $^{14}\text{C}$  signatures (small range of Fm), except for the highest temperature /  $E_a$   
 fractions of MOM and Bulk soil.

286 For the bulk soil and MOM fraction in the surface sample, and FPOM fractions at both depths, the C oxidized at the  
 lowest temperature had Fm >1, indicating that a portion of the C in the fraction was fixed mostly in the last 60 years.  
 For the FPOM fractions with Fm >1,  $^{14}\text{C}$  values are not as simply related to 'age' of the C. For example, the most

288 recently fixed C could have lower values than the mean, but so could older C if that is a mixture of pre-and post-  
bomb C. For all samples other than FPOM, the decline in  $F_m$   $^{14}\text{C}$  indicates a clear trend of increasing age (decreasing  
290  $F_m$ , indicating more time for radioactive decay of  $^{14}\text{C}$ ) especially at temperatures above that where most C was  
released (Figure 2). The highest-temperature thermal fractions ( $F_{max}$ , mostly 450 - 800°C, Appendix tables 1 and  
292 2) of surface bulk soil and MOM were similarly depleted in  $^{14}\text{C}$  and much older than any other values measured  
(Fig. 2).

294 In subsoils (30-50 cm), bomb  $^{14}\text{C}$  was found only in the FPOM fractions, so the decline in  $^{14}\text{C}$  with energy was  
determined mostly by the much lower  $^{14}\text{C}$  of C released at high temperatures (Figure 3). All fractions except the  
296 NaF Residue (NAF Res.) increased in  $F_m$  from the C collected in F1 and F2 (and F3 in bulk soil) temperature ranges  
(140-375°C), followed by decreases at increasingly higher temperatures. Excluding FPOM and OPOM, all fractions  
298 decreased significantly in  $F_m$  in  $F_{max}$  compared to the temperature range previous.

The chemical fractionation residues contained C with lower  $F_m$  than the unextracted MOM at all temperature ranges  
300 except in the highest temperature range collected. However, the highest temperature fraction collected for the MOM  
was greater (505 - 750°C), because insufficient C evolved from the chemical fraction residues in this range (Figure  
302 3). Thermograms for the chemical residues follow a similar pattern to those of MOM, with a small amount of  
younger but chemically resistant C released at low temperatures, and much older C released in  $F_{max}$ . As noted  
304 above, although the chemical residues contained less than 30% of the total MOM C (Table 1), their thermograms  
were very similar. The very old  $F_{max}$  thermal fractions in the chemical residues represent only a small amount (1-  
306 4%) of the total bulk soil C (Appendix tables 1 & 2).

### 308 3.3 $\delta^{13}\text{C}$

The  $\delta^{13}\text{C}$  of  $\text{CO}_2$  released from SOM generally increased with temperature in bulk soil and all fractions. The range  
310 of  $\delta^{13}\text{C}$  values from F1 to  $F_{max}$  was the greatest (increasing by 4-5‰) for the chemical residues, and smaller (3-  
4‰) for the density fractions. Across density fractions, the range of values and the differences in  $\delta^{13}\text{C}$  between  
312 different fractions was greater in the deeper soil layer. Interestingly, the FPOM at 30-50 cm was more enriched in  
 $^{13}\text{C}$  than OPOM. At high temperatures subsoil  $\delta^{13}\text{C}$  was generally more enriched than surface soil.

314

### 3.4 Contributions of different physical fractions to the thermal oxidation of bulk SOM

316 Thermograms (Figure 1) demonstrate that C released by the bulk sample at all temperatures contains C contributed  
from all physical and chemical fractions. For example, of the bulk C released in the temperature range where most  
318 C was released (250 to 325°C), FPOM and OPOM contributed 9% and 6%, respectively, of total C released in  
surface soil, and 16% and 8% in subsoil (Table 1, Fig. 1a). However, at higher temperature ranges, while the total  
320 C released was small (<5% of the total C) the proportional contribution from FPOM and OPOM fractions increased  
to ~40% in surface and 30% in subsoil (Figure 1c).

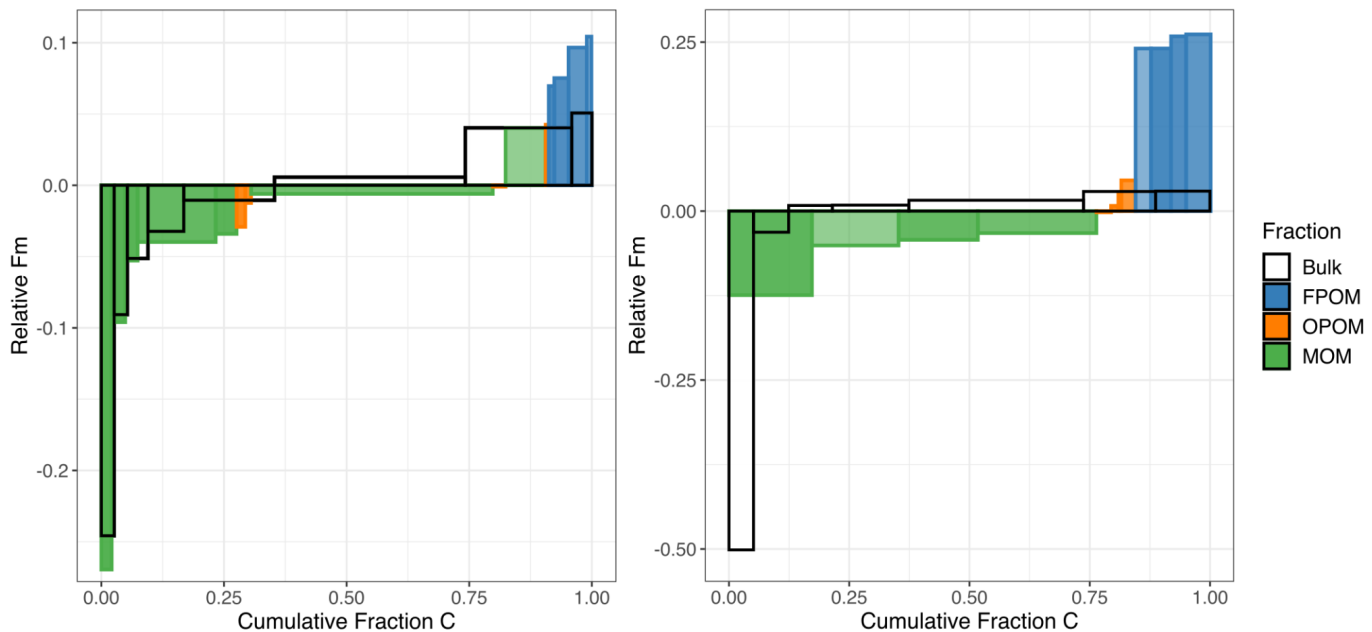
322

324 Thus, each thermal fraction from a combusted bulk soil contains C with a broad range of Fm and  $^{13}\text{C}$ , with variable  
326 contributions from the different physically fractionated components. Figure 5 summarizes the Fm distribution of C  
across the density and thermal fractions, and emphasizes that the difference of Fm between density fractions  
(especially FPOM versus MOM) is greater than the range of Fm within any individual density fraction (excluding a  
small amount of very old MOM) released as a function of temperature or  $E_a$  (Figure 5).

328 The measured distribution of  $^{14}\text{C}$  for C released with increasing temperature from the bulk soil clearly does not  
330 capture the contribution of FPOM with high Fm, because its young C is released across the same temperature ranges  
as other density and chemical fractions (Figs. 1a, 1c, 3, 4). Thus, the surface soil age distribution misses the ~9% of  
332 total C in FPOM that has a much higher  $^{14}\text{C}$  signature than bulk soil; instead, its contributions skew the bulk soil  
thermal  $^{14}\text{C}$  (Figure 5, wide bars in the middle of the distribution) higher than the separated MOM thermal fractions  
334 (green). This difference is even more pronounced in the subsoil.

336 With a sufficient number of thermal fractions at high temperatures, thermal analysis of the bulk soil C captured the  
small percentage of C with very depleted  $^{14}\text{C}$  signatures better than the chemical fractions that still mixed younger  
338 and older constituents. In surface soil, bulk soil  $F_{max}$   $^{14}\text{C}$  values (Fm 0.75) were comparable to  $F_{max}$  fractions of  
NaF Res. and  $\text{H}_2\text{O}_2$  Res. (Fm 0.76 and 0.78, respectively), and represented similar amounts of C (2.6%, 2.7%, and  
340 3.0% of total C, respectively) (Appendix table 1). Bulk subsoil  $F_{max}$  isolated older C (Fm 0.32, 5% of total C) than  
 $F_{max}$  values of NaF and  $\text{H}_2\text{O}_2$  residues (Fm 0.56, 8.1% total C and Fm 0.41, 3.8% total C, respectively), but high-  
342 temperature samples were not collected for these fractions because of low C yield (Appendix table 2).

344



346 **Figure 5:** Comparison of the cumulative Fm distribution of C released during thermal fractionation of bulk soil  
 348 versus oxidation of physically and chemically separated density fractions in the topsoil (left; 0-10cm) and subsoil  
 350 (right; 30-50cm). The height of each histogram element represents the Fm <sup>14</sup>C, normalized to the overall bulk Fm  
 352 value. Effectively, values above 0 contain more <sup>14</sup>C than bulk soil, and values below 0 contain less. The width of  
 354 bars corresponds to the proportion of total soil C in the fraction. The unfilled histogram elements (no color) represent  
 thermal fractions from the bulk soil, while the colored bars represent the thermally fractionated FPOM, OPOM and  
 MOM fractions shown in previous figures. Darker colors within a fraction correspond to higher temperature / *E<sub>a</sub>*  
 fractions, and lighter colors reflect cooler / lower *E<sub>a</sub>* fractions. Both are ordered by the <sup>14</sup>C content, with lowest on  
 the left and highest on the right.

356 **4 Discussion**

358 A main goal of this work is to compare the thermal oxidation profiles and <sup>14</sup>C age structures of thermally fractionated  
 360 SOM with more frequently applied physical (density) and chemical separation methods in a Podzol at two depths.  
 362 It is critical to find methods to quantify the age distribution of C in SOM, both to relate its persistence to processes  
 operating in soil, and to provide better constraints for testing models of soil C cycling. While density and chemical  
 fractions have proved useful, thermal fractionation offers the advantages of being less expensive and allowing for  
 rapid analysis of the total sample C content. Based on our results, we suggest that separation of FPOM followed by  
 thermal analysis provides the best characterization of the <sup>14</sup>C (age) distribution of C in SOM.

364

**4.1 Activation energy can predict age within a fraction but not between fractions**

366 Thermal fractionation of bulk soils and component physically- and chemically-separated SOM fractions demonstrate  
 that increased thermal stability (i.e., higher *E<sub>a</sub>*) is associated with lower radiocarbon (<sup>14</sup>C) content (i.e., older C ages;

368 Fig. 3), and more enriched  $^{13}\text{C}$  content (i.e., more microbially processed; Fig. 4). This supports the general  
assumptions of thermal analysis: that older and more microbially processed/degraded C will be released with  
370 increasing temperatures, even among fractions like FPOM that are not associated with minerals (Plante et al., 2009).  
Because there are large differences in  $F_m$  between the physically and chemically separated fractions, C released  
372 with similar activation energies (i.e., in a given thermal fraction of bulk soil) therefore can mix C with very different  
chemistry and  $^{14}\text{C}$  age.

374  
For example, particulate fractions FPOM and OPOM that contain fresh plant material as well as microbial residues  
376 (Castanha et al., 2008; Angst et al., 2021), release C across a similar temperature range as MOM. While presumably  
'labile', FPOM releases C between 300 - 500°C, reflecting the temperatures required to oxidize molecules like  
378 cellulose that make up plant material (Dahiya and Rana, 2004; Plante et al., 2009). Despite a range of activation  
energies,  $\delta^{13}\text{C}$  signatures (Fig. 4), and high  $\sigma E$  (Table 1) all suggesting chemical diversity, FPOM in this soil is all  
380 recent in origin (post-bomb,  $F_m > 1.0$ ) (Fig. 3) and typically breaks down within decades. Because of the temporal  
dynamics of the bomb spike, an increase or decrease in  $F_m$  is more difficult to associate directly to specific age for  
382 FPOM, and it is difficult to associate  $E_a$  directly to  $^{14}\text{C}$  values.

384 Mineral associated organic matter (MOM) fractions demonstrated larger though mostly overlapping ranges of  $E_a$ ,  
but released  $^{14}\text{C}$ -depleted and  $^{13}\text{C}$ -enriched C above 165  $\text{kJ mol}^{-1}$  (Figs. 2 - 4). For most MOM thermal fractions,  $F_m$   
386 less than 1.0 reflects the loss of  $^{14}\text{C}$  due to radioactive decay and therefore indicates an increase in age. Thus, within  
a given fraction there are predictable patterns of increasing age and  $\delta^{13}\text{C}$  with  $E_a$ . However, as found in other studies  
388 (Leifeld and von Lützow, 2014; Williams et al., 2018; Hemingway et al., 2019), these patterns do not allow  
prediction of age from  $E_a$  alone, highlighting fundamental differences in the processes controlling  $E_a$ ,  $^{14}\text{C}$  content,  
390 and age in each fraction. While  $E_a$  can either increase or decrease over time as C transforms with decomposition and  
recycling, the age of the involved C atoms can only increase.

392

#### 4.2 Age structure of MOM

394 Both chemical and thermal fractionation methods for MOM indicate the presence of two distinct components with  
very different  $F_m$ , one representing >95% of the C and having  $F_m$  similar to that of the bulk MOM but decreasing  
396 in  $^{14}\text{C}$  with increasing  $E_a$ , and a small amount (<5%) of much older C. In this Podzol, the main stabilization  
mechanisms are likely the interactions between percolating dissolved organic matter and pedogenic (oxy)hydroxides  
398 that could explain the large amount of relatively younger C (decades to centuries) removed by NaF and  $\text{H}_2\text{O}_2$  (Figure  
1b) that represents the largest thermal fraction of the MOM (F2). As shown by Schrumpf et al. (2021), the chemical  
400 extraction and oxidation of MOM using NaF and  $\text{H}_2\text{O}_2$ , respectively, removed C that was slightly higher in  $^{14}\text{C}$   
concentration than the MOM overall, leaving smaller but much older residues that resist destabilization. The majority  
402 of MOM-C removed through chemical fractionation had similar, younger ages that could reflect SOM more weakly  
associated with mineral surfaces, while the small proportion remaining could have been trapped within the mineral  
404 structure (e.g., in clays on formation) or represent elemental C. Both methods support the idea put forward by

406 Schrumpf et al. (2021) that much of the MOM was cycling on decadal timescales while a small amount (<10%) was  
much older (Fm 0.628). However, thermal methods demonstrate that the 3% of subsoil MOM oxidized at  
temperatures greater than 505°C was even older (Fm 0.23, Fig. 3, Table A1).

408  
410 While NaF and H<sub>2</sub>O<sub>2</sub> treatments removed younger C, combustion of the residues showed that they still contained C  
with a range of activation energies and ages. The chemical methods used here are believed to only remove sorbed C  
that likely has higher Fm (i.e., is younger) than the residue (Kaiser et al., 2007; Mikutta and Kaiser, 2011). These  
412 results are somewhat puzzling, as particularly the H<sub>2</sub>O<sub>2</sub> treatment is expected to remove all easily oxidizable C,  
leaving behind C that is either isolated or highly “recalcitrant”. We therefore expected that the H<sub>2</sub>O<sub>2</sub> residue would  
414 not only be older, but also on average have higher *E<sub>a</sub>*. On the contrary, there was actually proportionally less C in  
*F<sub>max</sub>* for both residues compared to the unextracted MOM (Figure 1, 3), such that the oldest C in the residues was  
416 likely mixed with younger C. The observation that H<sub>2</sub>O<sub>2</sub> residues had a range of activation energies and <sup>14</sup>C ages  
could indicate incomplete chemical oxidation or interaction of the OM associated with dissolved pedogenic phases  
418 with the remaining mineral phases. Alternatively, the presence of low *E<sub>a</sub>* material with very low <sup>14</sup>C could reflect  
incorporation of sedimentary shale parent material C into microbial food webs with long-term stabilization of  
420 microbial residues (Seifert et al., 2013).

422 Understanding the nature of the small amount of very old C found in MOM and bulk soil, and explaining the age  
and δ<sup>13</sup>C structure of the NaF and H<sub>2</sub>O<sub>2</sub> residue thermal fractions, requires additional information. One possibility  
424 is that the oldest C persists in the form of charcoal (Cusack et al., 2012; Sanderman et al., 2016) or is derived from  
the shale parent material of the Wetzstein site (Schrumpf et al., 2011; Grant et al., 2023). Unpublished <sup>14</sup>C data  
426 collected from the surface of rock fragments found in the soil indicate a Fm of 0.27, similar to values calculated for  
subsoil MOM *F<sub>max</sub>* fractions (Table 1). The thermal alteration of sedimentary parent material during metamorphism  
428 could also explain the chemical recalcitrance, heavier δ<sup>13</sup>C, and higher activation energies of this very old C. A  
second possibility is the presence of non-crystalline minerals that are often correlated with the amount of very old  
430 C found in soil (Huang et al., 2016; Khomo et al., 2017; Heckman et al., 2018a). The investigated soils have moderate  
oxalate extractable Fe contents of 9.2 (0-10 cm) and 17.4 (30-50 cm) g kg<sup>-1</sup> (Schrumpf et al. 2021 Biogeosciences,  
432 supplement). Dithionite extractable Fe concentrations (including both crystalline and non-crystalline components)  
were 17 and 27.4 g kg<sup>-1</sup> (respectively). However, quantifying such effects would require investigation of soils with  
434 varying amounts of non-crystalline minerals. A third explanation of long SOM persistence is the stochastic nature  
of the decomposition process. Available C is not uniformly decomposed, and some substrate may persist in soil on  
436 much longer timescales (Bolin and Rodhe, 1973; Bosatta and Ågren, 1985; Sierra et al., 2018). Through random  
chance associated with biological, chemical, and physical processes, a small portion of total SOM remains in soil  
438 for centuries to millennia. Such persistent C may be associated with the high activation energies measured here.

#### 440 **4.3 Suggested procedure for measuring the $^{14}\text{C}$ distribution of organic C in bulk soils**

441 The goal of any fractionation scheme for  $^{14}\text{C}$  analysis is to provide clearer delineation of C ages in soil, which  
442 integrates multiple types of SOM and stabilization mechanisms. Combining operationally-defined fractionation  
443 methods can further isolate distinct pools of C with varying  $^{14}\text{C}$  ages. Such age distributions can be used to constrain  
444 models of SOM dynamics (Sierra et al., 2014; Metzler et al., 2018; Chanca et al., 2022), and test hypotheses linking  
445 stabilization mechanisms with rates of C cycling. Overall, Figure 5 demonstrates that density fractionation alone  
446 cannot quantify age structure of bulk SOM, especially of MOM, while thermal fractionation of bulk SOM fails to  
447 capture the youngest part of the age distribution. This is because the youngest component of the soil C, the low  
448 density FPOM, releases C across nearly the entire range of combustion temperatures (Fig. 1c), making the C released  
449 from bulk soil at the lowest temperature reflect  $^{14}\text{C}$  ages that are too old, and the C released at higher temperatures  
450 too young. At the highest temperatures, however, thermal oxidation methods can isolate C even older than what can  
451 be found via aggressive chemical extractions (Fig 3). At the very highest temperatures, the contributions of C from  
452 oxidation of FPOM and OPOM are relatively small (Figs. 1c, 2) but may skew data with much younger C.

453  
454 In order to best capture the age distribution of C in SOM, we therefore recommend first separating the low density  
455 fraction, then applying thermal fractionation of the heavy fraction with attention to C liberated at very high  
456 temperatures to constrain and describe the age structure of MOM. As removal of the FPOM can also be accomplished  
457 using size separation, density separation may not be necessary if the main goal is to remove relatively fresh plant  
458 material (Castanha et al., 2008; Lavallee et al., 2020). However, the presence of charcoal that would be removed by  
459 density but not size could complicate the interpretation of thermal fractions, and further work is needed to resolve  
460 this special circumstance.

461  
462 Describing the distribution of ages in SOM is a powerful tool for testing hypotheses about the timescales of different  
463 C stabilization mechanisms in soils, and for comparison with age distributions produced by multi-compartment  
464 models (Metzler et al., 2018; Chanca et al., 2022). Our results are for a single soil, a Podzol that likely has one major  
465 mechanism for stabilizing C on mineral surfaces: interaction with pedogenic oxides. To explore other mineral  
466 stabilization mechanisms and timescales, it would be useful to compare thermograms and age distributions for soils  
467 with different mineral composition - e.g., allophane, 2:1 clays, 1:1 clays, sands, and as well as mixed mineralogy  
468 soils. Additionally, comparison with temperature-resolved spectra (e.g., py-GC/MS, (Sanderman and Grandy, 2020),  
469 DRIFTS (Nkwain et al., 2018), etc.) that associate SOM chemistry with thermal stability may help to determine the  
470 roles that OM chemistry and mineralogy play in controlling C age and persistence in soil.

#### 471 **5 Conclusions**

472 Each density and chemical fraction contained a spectrum of SOM ages. FPOM and OPOM displayed more  
473 homogeneous ages, while the MOM fraction displayed two distinct age components in this Podzol, identified in both  
474 top- and subsoil: likely the younger component that represents the majority of MOM stabilized by association with  
475 pedogenic (oxy)hydroxides, and the much older component possibly inherited from shale parent material.  
476

478 We conclude that thermal fractionation cannot completely replace standard fractionation methods to connect SOM  
properties (e.g., activation energy) to age distributions. Fresh FPOM contributes young C of homogenous age across  
480 temperatures up to 550°C and thus dilutes the signal of older C from other fractions. This method was effective at  
identifying multiple stabilization timescales on the MOM fraction, suggesting complex dynamics that may react  
482 across multiple timescales including those relevant to climate and management change. We thus recommend  
separating and measuring <sup>14</sup>C of FPOM, then analyzing thermal fractions of MOM to help distinguish faster- and  
484 slower-cycling mineral associated components. This additional fractionation helps to go beyond using mean <sup>14</sup>C  
values towards characterizing <sup>14</sup>C distributions that can provide a more comprehensive description of SOM cycling  
486 and potentially a more stringent test for models. Further efforts are needed to explore the effects of diverse mineral  
stabilization mechanisms on thermograms and <sup>14</sup>C distributions of MOM fractions.

488

#### **Data Availability**

490 Available via Github: [https://github.com/ShaneStoner/BGS\\_ThermalFractionation](https://github.com/ShaneStoner/BGS_ThermalFractionation) . The authors will acquire a  
DOI through Zenodo prior to publication.

492

#### **Acknowledgments**

494 This work was funded by the European Research Council (Horizon 2020 Research and Innovation Program; grant no.  
695101; 14Constraint) and the Max Planck Society. We gratefully acknowledge our reviewers who helped improve  
496 the manuscript. We thank Dr. Axel Steinhof and Dr. Xiaomei Xu for their invaluable assistance in developing the  
equipment and methods used in this study. We also thank the staff of the Max Planck Institute for Biogeochemistry,  
498 UC Irvine, and the Woods Hole Oceanographic Institute for their assistance in radiocarbon sampling and data  
preparation. Finally, we thank the CarboEurope Project for access to the archived soils used in this study.

500

#### **Author Contributions**

502 SWS and ST designed, constructed, and tested method hardware and protocols. Data were collected by SWS and  
analyzed by SWS and MS with input from all authors. SWS led the writing of the manuscript with significant  
504 contribution from ST and input from all authors.

506 **6 References**

- Anderson, D. W. and Paul, E. A.: Organo-Mineral Complexes and Their Study by Radiocarbon Dating, *Soil Science Society of America Journal*, 48, 298–301, <https://doi.org/10.2136/sssaj1984.03615995004800020014x>, 1984.
- 508 Angst, G., Mueller, K. E., Nierop, K. G. J., and Simpson, M. J.: Plant- or microbial-derived? A review on the  
510 molecular composition of stabilized soil organic matter, *Soil Biol Biochem*, 156, 108189,  
<https://doi.org/10.1016/j.soilbio.2021.108189>, 2021.
- 512 Baisden, W. T. and Canessa, S.: Using 50 years of soil radiocarbon data to identify optimal approaches for  
estimating soil carbon residence times, *Nucl Instrum Methods Phys Res B*, 294, 588–592,  
514 <https://doi.org/10.1016/j.nimb.2012.06.021>, 2013.
- Balesdent, J.: The turnover of soil organic fractions estimated by radiocarbon dating, *Science of the Total*  
516 *Environment*, The, 62, 405–408, [https://doi.org/10.1016/0048-9697\(87\)90528-6](https://doi.org/10.1016/0048-9697(87)90528-6), 1987.
- Basile-Doelsch, I., Balesdent, J., and Pellerin, S.: Reviews and syntheses: The mechanisms underlying carbon  
518 storage in soil, *Biogeosciences*, 17, 5223–5242, <https://doi.org/10.5194/bg-17-5223-2020>, 2020.
- Bianchi, T. S., Galy, V., Rosenheim, B. E., Shields, M., Cui, X., and Van Metre, P.: Paleoreconstruction of organic  
520 carbon inputs to an oxbow lake in the Mississippi River watershed: Effects of dam construction and land use  
change on regional inputs, *Geophys Res Lett*, 42, 7983–7991, <https://doi.org/10.1002/2015GL065595>, 2015.
- 522 Bolin, B. and Rodhe, H.: A note on the concepts of age distribution and transit time in natural reservoirs, *Tellus*, 25,  
58–62, <https://doi.org/10.1111/j.2153-3490.1973.tb01594.x>, 1973.
- 524 Bosatta, E. and Ågren, G. I.: Theoretical analysis of decomposition of heterogeneous substrates, *Soil Biol Biochem*,  
17, 601–610, [https://doi.org/10.1016/0038-0717\(85\)90035-5](https://doi.org/10.1016/0038-0717(85)90035-5), 1985.
- 526 Castanha, C., Trumbore, S., and Amundson, R.: Methods of separating soil carbon pools affect the chemistry and  
turnover time of isolated fractions, *Radiocarbon*, 50, 83–97, <https://doi.org/10.1017/S003822200043381>, 2008.
- 528 Chanca, I., Trumbore, S., Macario, K., and Sierra, C. A.: Probability Distributions of Radiocarbon in Open Linear  
Compartmental Systems at Steady-State, *J Geophys Res Biogeosci*, 127, 1–23,  
530 <https://doi.org/10.1029/2021JG006673>, 2022.
- De Coninck, F.: Major mechanisms in formation of spodic horizons, *Geoderma*, 24, 101–128, 1980.
- 532 Cotrufo, M. F., Ranalli, M. G., Haddix, M. L., Six, J., and Lugato, E.: Soil carbon storage informed by particulate  
and mineral-associated organic matter, *Nat Geosci*, 12, 989–994, <https://doi.org/10.1038/s41561-019-0484-6>,  
534 2019.
- Cusack, D. F., Chadwick, O. A., Hockaday, W. C., and Vitousek, P. M.: Mineralogical controls on soil black carbon  
536 preservation, *Global Biogeochem Cycles*, 26, 1–10, <https://doi.org/10.1029/2011GB004109>, 2012.
- Dahiya, J. B. and Rana, S.: Thermal degradation and morphological studies on cotton cellulose modified with  
538 various arylphosphorodichloridites, *Polym Int*, 53, 995–1002, <https://doi.org/10.1002/pi.1500>, 2004.
- Feng, X. and Simpson, M. J.: Temperature responses of individual soil organic matter components, *J Geophys Res*  
540 *Biogeosci*, 113, 1–14, <https://doi.org/10.1029/2008JG000743>, 2008.
- González-Pérez, J. A., Chabbi, A., de la Rosa, J. M., Rumpel, C., and González-Vila, F. J.: Evolution of organic  
542 matter in lignite-containing sediments revealed by analytical pyrolysis (Py-GC-MS), *Org Geochem*, 53, 119–  
130, <https://doi.org/10.1016/j.orggeochem.2012.08.001>, 2012.
- 544 Grandy, A. S., Strickland, M. S., Lauber, C. L., Bradford, M. A., and Fierer, N.: The influence of microbial  
communities, management, and soil texture on soil organic matter chemistry, *Geoderma*, 150, 278–286,  
546 <https://doi.org/10.1016/j.geoderma.2009.02.007>, 2009.
- Grant, K. E., Galy, V. V., Chadwick, O. A., and Derry, L. A.: Thermal oxidation of carbon in organic matter rich  
548 volcanic soils: insights into SOC age differentiation and mineral stabilization, *Biogeochemistry*, 144, 291–304,  
<https://doi.org/10.1007/s10533-019-00586-1>, 2019.
- 550 Grant, K. E., Hilton, R. G., and Galy, V.: Global patterns of radiocarbon depletion in subsoil linked to rock-derived  
organic carbon, *Geochem Perspect Lett*, 36–40, 2023.

552 Gregorich, E. G., Beare, M. H., McKim, U. F., and Skjemstad, J. O.: Chemical and Biological Characteristics of  
 554 Physically Uncomplexed Organic Matter, *Soil Science Society of America Journal*, 70, 975–985,  
<https://doi.org/10.2136/sssaj2005.0116>, 2006.

556 Heckman, K., Lawrence, C. R., and Harden, J. W.: A sequential selective dissolution method to quantify storage and  
 stability of organic carbon associated with Al and Fe hydroxide phases, *Geoderma*, 312, 24–35,  
<https://doi.org/10.1016/j.geoderma.2017.09.043>, 2018a.

558 Heckman, K., Throckmorton, H., Horwath, W., Swanston, C., and Rasmussen, C.: Variation in the Molecular  
 560 Structure and Radiocarbon Abundance of Mineral-Associated Organic Matter across a Lithosequence of Forest  
 Soils, *Soil Syst*, 2, 36, <https://doi.org/10.3390/soilsystems2020036>, 2018b.

562 Heckman, K., Hicks Pries, C. E., Lawrence, C. R., Rasmussen, C., Crow, S. E., Hoyt, A. M., von Fromm, S. F., Shi,  
 Z., Stoner, S., McGrath, C., Beem-Miller, J., Berhe, A. A., Blankinship, J. C., Keiluweit, M., Marín-Spiotta, E.,  
 564 Monroe, J. G., Plante, A. F., Schimel, J., Sierra, C. A., Thompson, A., and Wagai, R.: Beyond bulk: Density  
 fractions explain heterogeneity in global soil carbon abundance and persistence, *Glob Chang Biol*, 28, 1178–  
 1196, <https://doi.org/10.1111/gcb.16023>, 2022.

566 Helfrich, M., Flessa, H., Mikutta, R., Dreves, A., and Ludwig, B.: Comparison of chemical fractionation methods  
 for isolating stable soil organic carbon pools, *Eur J Soil Sci*, 58, 1316–1329, <https://doi.org/10.1111/j.1365-2389.2007.00926.x>, 2007.

568 Hemingway, J. D.: rampedpyrox: Open-source tools for thermoanalytical data analysis, 2016, 2017.

570 Hemingway, J. D., Rothman, D. H., Rosengard, S. Z., and Galy, V. V.: Technical note: An inverse method to relate  
 organic carbon reactivity to isotope composition from serial oxidation, *Biogeosciences*, 14, 5099–5114,  
 572 <https://doi.org/10.5194/bg-14-5099-2017>, 2017.

Hemingway, J. D., Rothman, D. H., Grant, K. E., Rosengard, S. Z., Eglinton, T. I., Derry, L. A., and Galy, V. V.:  
 574 Mineral protection regulates long-term global preservation of natural organic carbon, *Nature*, 570, 228–231,  
<https://doi.org/10.1038/s41586-019-1280-6>, 2019.

576 Huang, X., Jiang, H., Li, Y., Ma, Y., Tang, H., Ran, W., and Shen, Q.: The role of poorly crystalline iron oxides in  
 the stability of soil aggregate-associated organic carbon in a rice-wheat cropping system, *Geoderma*, 279, 1–10,  
 578 <https://doi.org/10.1016/j.geoderma.2016.05.011>, 2016.

Jagadamma, S., Lal, R., Ussiri, D. A. N., Trumbore, S. E., and Mestelan, S.: Evaluation of structural chemistry and  
 580 isotopic signatures of refractory soil organic carbon fraction isolated by wet oxidation methods,  
*Biogeochemistry*, 98, 29–44, <https://doi.org/10.1007/s10533-009-9374-0>, 2010.

582 Kaiser, K., Mikutta, R., and Guggenberger, G.: Increased Stability of Organic Matter Sorbed to Ferrihydrite and  
 Goethite on Aging, *Soil Science Society of America Journal*, 71, 711–719,  
 584 <https://doi.org/10.2136/sssaj2006.0189>, 2007.

586 Khomo, L., Trumbore, S., Bern, C. R., and Chadwick, O. A.: Timescales of carbon turnover in soils with mixed  
 crystalline mineralogies, *Soil*, 3, 17–30, <https://doi.org/10.5194/soil-3-17-2017>, 2017.

588 Kleber, M., Bourg, I. C., Coward, E. K., Hansel, C. M., Myneni, S. C. B., and Nunan, N.: Dynamic interactions at  
 the mineral–organic matter interface, *Nat Rev Earth Environ*, 0123456789, <https://doi.org/10.1038/s43017-021-00162-y>, 2021.

590 Lavalley, J. M., Soong, J. L., and Cotrufo, M. F.: Conceptualizing soil organic matter into particulate and mineral-  
 associated forms to address global change in the 21st century, *Glob Chang Biol*, 26, 261–273,  
 592 <https://doi.org/10.1111/gcb.14859>, 2020.

594 Lehmann, J. and Kleber, M.: The contentious nature of soil organic matter, *Nature*, 528, 60–68,  
<https://doi.org/10.1038/nature16069>, 2015.

596 Leifeld, J. and von Lützow, M.: Chemical and microbial activation energies of soil organic matter decomposition,  
*Biol Fertil Soils*, 50, 147–153, <https://doi.org/10.1007/s00374-013-0822-6>, 2014.

598 von Lützow, M., Kögel-Knabner, I., Ekschmitt, K., Flessa, H., Guggenberger, G., Matzner, E., and Marschner, B.:  
 SOM fractionation methods: Relevance to functional pools and to stabilization mechanisms, *Soil Biol Biochem*,  
 39, 2183–2207, <https://doi.org/10.1016/j.soilbio.2007.03.007>, 2007.

600 Metzler, H., Müller, M., and Sierra, C. A.: Transit-time and age distributions for nonlinear time-dependent  
602 compartmental systems, *Proc Natl Acad Sci U S A*, 115, 1150–1155, <https://doi.org/10.1073/pnas.1705296115>,  
2018.

Mikutta, R. and Kaiser, K.: Organic matter bound to mineral surfaces: Resistance to chemical and biological  
604 oxidation, *Soil Biol Biochem*, 43, 1738–1741, <https://doi.org/10.1016/j.soilbio.2011.04.012>, 2011.

Natali, C., Bianchini, G., and Carlino, P.: Thermal stability of soil carbon pools: Inferences on soil nature and  
606 evolution, *Thermochim Acta*, 683, 178478, <https://doi.org/https://doi.org/10.1016/j.tca.2019.178478>, 2020.

Nkwain, F. N., Demyan, M. S., Rasche, F., Dignac, M. F., Schulz, E., Kätterer, T., Müller, T., and Cadisch, G.:  
608 Coupling pyrolysis with mid-infrared spectroscopy (Py-MIRS) to fingerprint soil organic matter bulk chemistry,  
*J Anal Appl Pyrolysis*, 133, 176–184, <https://doi.org/10.1016/j.jaap.2018.04.004>, 2018.

Paul, E. A., Follett, R. F., Leavitt, S. W., Halvorson, A., Peterson, G. A., and Lyon, D. J.: Radiocarbon Dating for  
610 Determination of Soil Organic Matter Pool Sizes and Dynamics, *Soil Science Society of America Journal*, 61,  
612 1058–1067, <https://doi.org/10.2136/sssaj1997.03615995006100040011x>, 1997.

Plante, A. F., Fernández, J. M., and Leifeld, J.: Application of thermal analysis techniques in soil science,  
614 *Geoderma*, 153, 1–10, <https://doi.org/10.1016/j.geoderma.2009.08.016>, 2009.

Plante, A. F., Fernández, J. M., Haddix, M. L., Steinweg, J. M., and Conant, R. T.: Biological, chemical and thermal  
616 indices of soil organic matter stability in four grassland soils, *Soil Biol Biochem*, 43, 1051–1058,  
<https://doi.org/10.1016/j.soilbio.2011.01.024>, 2011.

Plante, A. F., Beaupré, S. R., Roberts, M. L., and Baisden, T.: Distribution of Radiocarbon Ages in Soil Organic  
618 Matter by Thermal Fractionation, *Radiocarbon*, 55, 1077–1083, <https://doi.org/10.1017/s0033822200058215>,  
620 2013.

Quénéa, K., Derenne, S., González-Vila, F. J., González-Pérez, J. A., Mariotti, A., and Largeau, C.: Double-shot  
622 pyrolysis of the non-hydrolysable organic fraction isolated from a sandy forest soil (Landes de Gascogne,  
South-West France): Comparison with classical Curie point pyrolysis, *J Anal Appl Pyrolysis*, 76, 271–279,  
624 <https://doi.org/10.1016/j.jaap.2005.12.007>, 2006.

Rasmussen, C., Throckmorton, H., Liles, G., Heckman, K., Meding, S., and Horwath, W. R.: Controls on soil  
626 organic carbon partitioning and stabilization in the California Sierra Nevada, *Soil Syst*, 2, 1–18,  
<https://doi.org/10.3390/soilsystems2030041>, 2018.

Rennert, T. and Herrmann, L.: Sea spray and land use effects on clay minerals and organic matter of soils on  
628 machair (Harris, Scotland), *Geoderma Regional*, 23, e00339, <https://doi.org/10.1016/j.geodrs.2020.e00339>,  
630 2020.

Rennert, T. and Herrmann, L.: Thermal-gradient analysis of soil organic matter using an elemental analyser – A tool  
632 for qualitative characterization?, *Geoderma*, 425, 116085, <https://doi.org/10.1016/j.geoderma.2022.116085>,  
2022.

Rosenheim, B. E. and Galy, V.: Direct measurement of riverine particulate organic carbon age structure, *Geophys  
634 Res Lett*, 39, 1–6, <https://doi.org/10.1029/2012GL052883>, 2012.

Rosenheim, B. E., Day, M. B., Domack, E., Schrum, H., Benthien, A., and Hayes, J. M.: Antarctic sediment  
636 chronology by programmed-temperature pyrolysis: Methodology and data treatment, *Geochemistry,  
638 Geophysics, Geosystems*, 9, 1–16, <https://doi.org/10.1029/2007GC001816>, 2008.

Sanderman, J. and Grandy, S. A.: Ramped thermal analysis for isolating biologically meaningful soil organic matter  
640 fractions with distinct residence times, *Soil*, 6, 131–144, <https://doi.org/10.5194/soil-6-131-2020>, 2020.

Sanderman, J., Baisden, W. T., and Fallon, S.: Redefining the inert organic carbon pool, *Soil Biol Biochem*, 92,  
642 149–152, <https://doi.org/10.1016/j.soilbio.2015.10.005>, 2016.

Schrumpf, M., Schulze, E. D., Kaiser, K., and Schumacher, J.: How accurately can soil organic carbon stocks and  
644 stock changes be quantified by soil inventories?, *Biogeosciences*, 8, 1193–1212, <https://doi.org/10.5194/bg-8-1193-2011>, 2011.

Schrumpf, M., Kaiser, K., Guggenberger, G., Persson, T., Kögel-Knabner, I., and Schulze, E. D.: Storage and  
646 stability of organic carbon in soils as related to depth, occlusion within aggregates, and attachment to minerals,  
648 *Biogeosciences*, 10, 1675–1691, <https://doi.org/10.5194/bg-10-1675-2013>, 2013.

650 Schrumpf, M., Kaiser, K., Mayer, A., Hempel, G., and Trumbore, S.: Age distribution, extractability, and stability of  
mineral-bound organic carbon in central European soils, *Biogeosciences*, 18, 1241–1257,  
<https://doi.org/10.5194/bg-18-1241-2021>, 2021.

652 Schuur, E. A. G., Trumbore, S. E., and Druffel, E. R. M.: Radiocarbon and Climate Change: Mechanisms,  
Applications and Laboratory Techniques, 1–315 pp., <https://doi.org/10.1007/978-3-319-25643-6>, 2016.

654 Seifert, A. G., Trumbore, S., Xu, X., Zhang, D., and Gleixner, G.: Variable effects of plant colonization on black  
slate uptake into microbial PLFAs, *Geochim Cosmochim Acta*, 106, 391–403,  
<https://doi.org/10.1016/j.gca.2012.12.011>, 2013.

656 Sierra, C. A., Müller, M., and Trumbore, S. E.: Modeling radiocarbon dynamics in soils: SoilR version 1.1, *Geosci  
Model Dev*, 7, 1919–1931, <https://doi.org/10.5194/gmd-7-1919-2014>, 2014.

658 Sierra, C. A., Hoyt, A. M., He, Y., and Trumbore, S. E.: Soil Organic Matter Persistence as a Stochastic Process:  
Age and Transit Time Distributions of Carbon in Soils, *Global Biogeochem Cycles*, 32, 1574–1588,  
<https://doi.org/10.1029/2018GB005950>, 2018.

662 Sollins, P., Kramer, M. G., Swanston, C., Lajtha, K., Filley, T., Aufdenkampe, A. K., Wagai, R., and Bowden, R.  
D.: Sequential density fractionation across soils of contrasting mineralogy: Evidence for both microbial- and  
664 mineral-controlled soil organic matter stabilization, *Biogeochemistry*, 96, 209–231,  
<https://doi.org/10.1007/s10533-009-9359-z>, 2009.

666 Torn, M. S., Trumbore, S. E., Chadwick, O. A., Vitousek, P. M., and Hendricks, D. M.: Mineral control of soil  
organic carbon and storage and turnover, *Nature*, 389, 3601–3603, 1997.

668 Trumbore, S.: Age of soil organic matter and soil respiration: Radiocarbon constraints on belowground C dynamics,  
*Ecological Applications*, 10, 399–411, [https://doi.org/10.1890/1051-0761\(2000\)010\[0399:AOSOMA\]2.0.CO;2](https://doi.org/10.1890/1051-0761(2000)010[0399:AOSOMA]2.0.CO;2),  
670 2000.

Trumbore, S. E.: Comparisons of carbon dynamics in tropical and temperate soils using radiocarbon measurements,  
672 *Measurement*, 7, 275–290, 1993.

Trumbore, S. E. and Zheng, S.: Comparison of fractionation methods for soil organic matter <sup>14</sup>C analysis, 38, 219–  
674 229, 1996.

Trumbore, S. E., Bonani, G., and Wolfli, W.: The rates of carbon cycling in several soils from AMS<sup>14</sup>C  
676 measurements of fractionated soil organic matter, John Wiley and Sons Inc, United States, 1990.

Wendeberg, M., Richter, J. M., Rothe, M., and Brand, W. A.: Jena Reference Air Set (JRAS): A multi-point scale  
678 anchor for isotope measurements of CO<sub>2</sub> in air, *Atmos Meas Tech*, 6, 817–822, <https://doi.org/10.5194/amt-6-817-2013>, 2013.

680 Williams, E. K., Fogel, M. L., Berhe, A. A., and Plante, A. F.: Distinct bioenergetic signatures in particulate versus  
mineral-associated soil organic matter, *Geoderma*, 330, 107–116,  
682 <https://doi.org/10.1016/j.geoderma.2018.05.024>, 2018.

Xu, X., Trumbore, S. E., Zheng, S., Southon, J. R., McDuffee, K. E., Luttgen, M., and Liu, J. C.: Modifying a sealed  
684 tube zinc reduction method for preparation of AMS graphite targets: Reducing background and attaining high  
precision, *Nucl Instrum Methods Phys Res B*, 259, 320–329, <https://doi.org/10.1016/j.nimb.2007.01.175>, 2007.

686